IN-90
058412

COLLIDE: Collisions Into Dust Experiment
Final Report

May 5, 1999

Principal Investigator and Payload Manager:
Joshua E. Colwell
Laboratory for Atmospheric and Space Physics
University of Colorado
Campus Box 392
Boulder CO 80309-0392

NASA Grants: NAGW-4843, NAG5-3708, NAG3-2071

The Collisions Into Dust Experiment (COLLIDE) was completed and flew on STS-90 in April and May of 1998. After the experiment was returned to Earth, the data and experiment were analyzed. Some anomalies occurred during the flight which prevented a complete set of data from being obtained. However, the experiment did meet its criteria for scientific success and returned surprising results on the outcomes of very low energy collisions into powder.

The attached publication, "Low Velocity Microgravity Impact Experiments into Simulated Regolith," describes in detail the scientific background, engineering, and scientific results of COLLIDE. Our scientific conclusions, along with a summary of the anomalies which occurred during flight, are contained in that publication. We offer it as our final report on this grant.

Icarus 138, 241–248 (1999)
Article ID icar.1998.6073, available online at http://www.idealibrary.com on IDEAL®

Low-Velocity Microgravity Impact Experiments into Simulated Regolith

Joshua E. Colwell

Laboratory for Atmospheric and Space Physics, University of Colorado, Campus Box 392, Boulder, Colorado 80309-0392
E-mail: colwell@casper.colorado.edu

and

Martin Taylor

Space Telescope Science Institute, RPO, 3700 San Martin Drive, Baltimore, Maryland 21218

Received August 10, 1998; revised November 23, 1998

We describe the Collisions Into Dust Experiment (COLLIDE), a microgravity experiment to study the outcome of very low velocity (1–100 cm/sec) collisions into a simulated regolith. The experiment was flown on the Space Shuttle in April 1998 and included six independent impact experiments into a lunar soil simulant. Results of these impact experiments showed very little dust ejecta was produced in the impacts, which were highly inelastic. We present normal and tangential coefficients of restitution for impacts into simulated regolith at speeds between 15 and 90 cm/sec. We find normal coefficients of restitution of 2 to 3%, significantly lower than is suggested by extrapolation from low-velocity impact experiments with ice, but consistent with higher velocity impacts into powder. Our microgravity experiment confirms the ground-based result of Hartmann (1978, *Icarus* 33, 50–62) that the presence of a regolith increases the efficiency of planetary accretion. The absence of dust ejecta suggests higher energy collisions are necessary to release the dust observed in planetary rings.

Key Words: planetary rings; planetesimals; experimental techniques; dust; collisions.

I. INTRODUCTION

Collisions between planetary ring particles and in some protoplanetary disk environments occur at low impact velocities ($v < 1$ m/sec). In some regions of Saturn's rings, for example, the typical collision velocity inferred from observations by the Voyager spacecraft and dynamical modeling is a fraction of a centimeter per second (Esposito 1993). Although no direct observations of an individual ring particle exist, the abundance of dust in planetary rings and protoplanetary disks suggests that larger ring and disk particles are coated with a layer of smaller particles and dust—the "regolith." Because the ring particles and proto-planetesimals are small (cm to m-sized), the regolith is only weakly bound to the surface by gravity. COLLIDE provides microgravity impact experiments to complement the extensive set of ground-based experimental data.

Low-velocity impact experiments simulating planetary ring particle collisions have been performed by Bridges *et al.* (1984), Hatzes *et al.* (1988), Supulver *et al.* (1995), and Dilley and Crawford (1996) using hard ice particles and pendulums to achieve impact velocities less than 1 cm/sec, typical of planetary ring particle impact velocities. Although Hatzes *et al.* (1988) used frosted ice impactors, there was no unconsolidated regolith. Hartmann (1978) performed impact experiments onto bare rock and into regolith at speeds down to 1.4 m/sec and found that the presence of a regolith favors accretion by substantially decreasing the rebound velocity. The terrestrial gravitational environment prevented any significant ejecta production in those low-velocity impacts. Further experiments by Hartmann (1985) included impact velocities as low as 5.3 m/sec into regolith and produced measurable amounts of regolith ejecta. Ryan *et al.* (1991) performed drop experiments and pendulum impacts at speeds down to 0.6 m/sec and found that the presence of a regolith inhibited the fragmentation of aggregate bodies, but no data on ejecta from the regolith targets were presented.

Ejecta from regolith on ring particles is presumably the source of dust in most planetary rings. The regolith is generated by the ongoing bombardment of the larger "parent" particles by the interplanetary micrometeoroid flux. Dust is released by micrometeoroid impacts, which occur at speeds of many kilometers per second and by much slower interparticle collisions, resulting in dust rings. However, the amount of dust released in the slower collisions and the velocity distribution of the ejecta is unknown. The dominant loss process for dust in at least some dust rings is reaccreation by the larger particles (e.g., Colwell and Esposito 1990a). The regolith of the large particles can therefore act as a reservoir for the visible dust rings. The size and velocity distributions of the macroscopic ring particles have been inferred from the dust optical depth (Colwell and Esposito 1990a, 1990b).

0019-1035/99 $30.00

These inferences were based in part on extrapolations of impact experiments performed in a terrestrial gravity environment with impact speeds in excess of 1 km/sec to the cm/sec velocity range. Our experiments provide data on the release of dust from ring particle regoliths in low-velocity collisions. Regolith ejecta was produced in 5 m/sec (and higher) ground-based impact experiments (Hartmann 1985); the experiments presented here are an extension of those to a microgravity environment and impact speeds of less than 1 m/sec.

Similar types of collisions were likely involved in the early stages of planet formation. These collisions likely occurred at relative velocities of 1–100 cm/sec for either a laminar or turbulent nebula (Weidenschilling and Cuzzi 1993), and low velocities persisted even for objects as large as a kilometer in radius (Barge and Pellat 1991). Velocities less than 1 m/sec are significantly higher than escape velocities for centimeter-to-meter size particles, and so collisions must have been highly inelastic in order for growth to proceed. Dusty regoliths covering particles may have helped to dissipate collisional energy, reducing the rate of mass loss during collisions and promoting accretional growth of larger bodies. Although accretion is inhibited in planetary rings by tidal forces, limited accretion can occur, particularly if the accreting particles do not have comparable masses, resulting in temporary aggregates which persist until a particularly energetic collision disrupts it (Weidenschilling *et al.* 1984, Canup and Esposito 1995). Accretion in this environment also involves low-velocity collisions between dust-covered objects.

The same kind of gentle collisions that occurred in the early stages of planetesimal accretion may still be occurring in the outer regions of the Solar System in the Kuiper Belt. Collision velocities are much lower in the Kuiper Belt than in the Asteroid Belt, but the system is collisionally evolved (Stern 1996a). The Kuiper Belt population of primordial Solar System objects may extend well beyond 50 AU, where gravitational perturbations from the giant planets are small (Stern and Colwell 1997). At these large heliocentric distances, even moderate eccentricities result in relatively low impact speeds (tens to hundreds of m/sec) compared to the several kilometers per second impact speeds in the asteroid belt. The release of dust from such collisions in extra-solar analogs to the Kuiper Belt may be detectable in infrared observations of other planetary systems (Stern 1996b). Such low-energy collisions may also be responsible for the steady-state distribution of dust in observed protoplanetary disks, such as the Beta Pictoris disk, and interstellar dust (e.g., Greenberg *et al.* 1978).

The Collisions Into Dust Experiment (COLLIDE) was designed to study the partitioning of energy in low-speed collisions into a regolith in a microgravity environment, such as occurs in planetary rings and protoplanetary disks. In the next section we describe the experimental procedure, and in Section III we present results from the first flight of COLLIDE. We conclude with a discussion of the implications of the results on planetary ring and protoplanetary disk dynamics.

II. EXPERIMENTAL PROCEDURE

In order to study low-velocity collisions into a dust-covered surface such as those that occur between small particles in space, a microgravity environment is necessary. COLLIDE is a Get Away Special (GAS) payload for the Space Transportation System (Space Shuttle). It is a self-contained experiment consisting of six independent collision experiments allowing for six different sets of impact parameters to be studied in a single flight (Fig. 1). Each impact takes place in a self-contained and independent Impactor Box System (IBS, Fig. 2). Science data were stored on two digital video tapes recorded by digital video camcorders inside the experiment. Projectiles were 3/8 inch and 3/4 inch diameter Teflon spheres launched by springs at speeds between 1 and 100 cm/sec, depending on the IBS. Teflon was chosen to minimize internal friction in the launcher mechanism and because its density (2.2 g/cm^3) is similar to icy-silicate mixtures. The target was a tray of JSC-1 powder, sifted through a no. 60 (246 micrometer) sieve. JSC-1 is a glass-rich basaltic ash which has chemical composition, mineralogy, particle size distribution, and engineering properties similar to lunar mare regolith (McKay *et al.* 1994). The depths of the target trays were 3/8 inch and 3/4 inch, depending on the IBS, and the trays were filled with JSC-1 prior to launch. Minimal filling of the target trays under 1 Earth gravity corresponds to a relative density, $D_r = 0$, where relative density is defined by

$$D_r = \frac{e_{max} - e}{e_{max} - e_{min}}. \quad (1)$$

A relative density of 1 corresponds to the density of the material achieved following vibration with a compressive force on the material. The material constants e_{max} and e_{min} are determined experimentally by measuring void ratios of the material following compression and vibration (e_{max}) and with no load applied (e_{min}). On COLLIDE, the amount of JSC-1 in the target tray corresponded to relative densities between 27 and 33%, set by the fixed volume of the target tray and the masses of JSC-1 loaded into the trays prior to launch. The void ratio, e, is the volume of voids divided by the volume of solids,

$$e = \frac{G_s \rho_w}{\rho_d} - 1, \quad (2)$$

where G_s is the specific gravity of the material, ρ_w is the density of water, and ρ_d is the bulk density of the sample. The void ratio is related to the porosity, n, by $n = e/(1 + e)$. For JSC-1, $G_s = 2.9$, $e_{max} = 1.028$, and $e_{min} = 0.585$. The bulk densities, void ratios, and porosities for each IBS are included in Table I along with designed impact parameters. For comparison, the porosity of the top 1 cm of lunar regolith is 0.59, corresponding to a bulk density of 1.4 g/cm^3, based on interpretation of microwave observations during a lunar eclipse (Sandor and Clancy 1995).

Each IBS was mounted so that the camcorder viewed the target surface edge-on, and impacts were perpendicular to the target

TABLE I
Experimental Parameters

IBS	1	2	3	4	5	6
Parameter						
Designed impact speed (cm/sec)	4.64	21.5	100	21.5	1.0	100
Projectile radius (cm)	0.48	0.48	0.96	0.48	0.48	0.48
Projectile mass (g)	0.99	0.99	7.9	0.99	0.99	0.99
Target depth (cm)	1.9	0.95	1.9	1.9	1.9	1.9
Target void ratio	0.90	0.88	0.91	0.90	0.90	0.91
Target relative density	0.29	0.33	0.27	0.29	0.28	0.27
Target bulk density (g/cm3)	1.53	1.54	1.52	1.53	1.52	1.52
Target porosity	0.47	0.47	0.48	0.47	0.47	0.48

surface. A mirror was mounted on the bottom of each IBS to provide an orthogonal view of the impact. The IBSs are made of aluminum with clear polycarbonate tops to allow video recording. Illumination for the camcorders was provided by high-intensity light emitting diodes (LEDs). The target dust was held in place by a door on a motorized assembly. The dimensions of the target surface were 10.5 by 11.0 cm. The six IBSs were run in sequence, with each of two camcorders viewing three IBSs. The activity sequence for each IBS is the same. The camcorder begins recording. The LEDs are turned on. A digital linear actuator (stepper motor) operates, sliding the door across the surface of the target dust and out of the way of the impactor, revealing the target surface to the projectile. A shape memory alloy circuit is activated resulting in release of the spring-launched projectile into the target tray. The camcorder operates for an additional 30 to 180 sec, depending on the IBS, recording the effects of the collision. Complete execution of the experiment takes 22 min 31 sec.

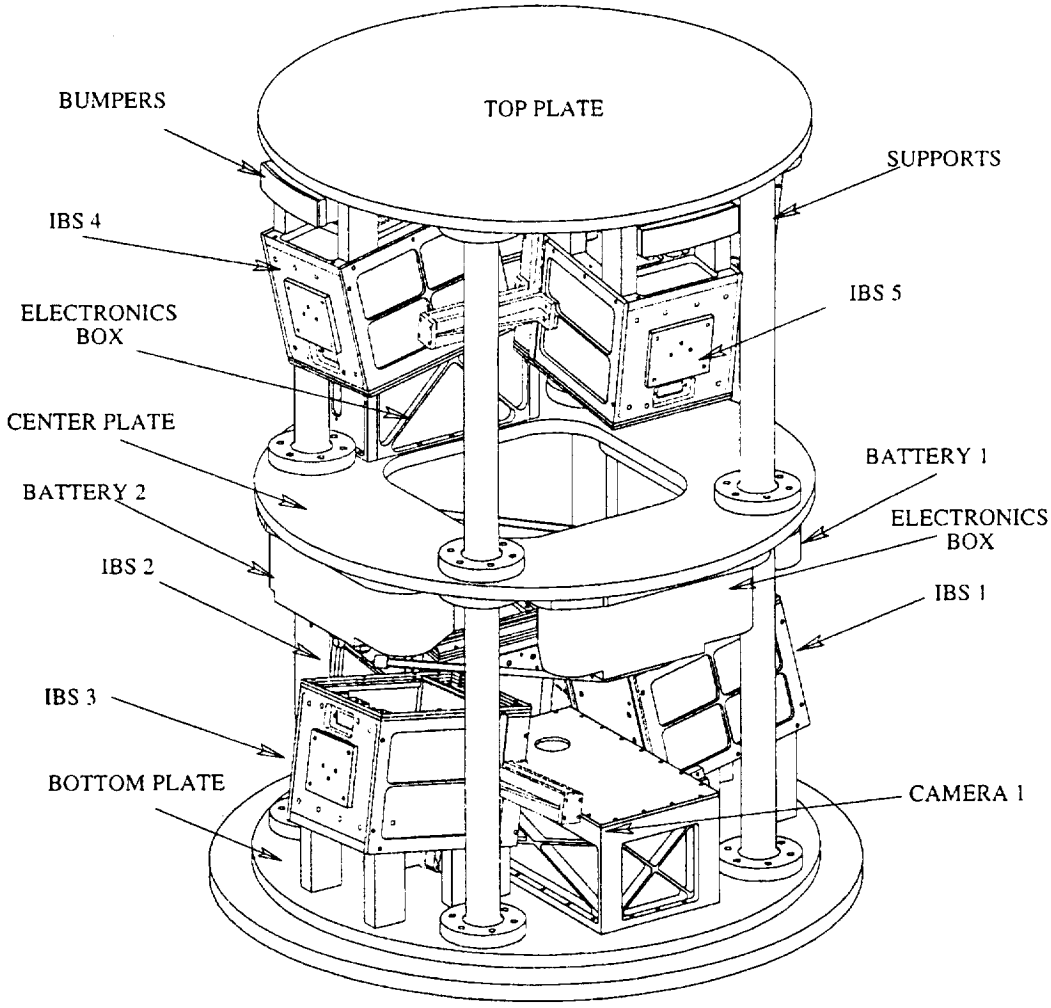

FIG. 1. The Collisions Into Dust Experiment (COLLIDE) main structure and components. A camcorder is mounted on each end plate, top and bottom, along with three Impactor Box Systems (IBS). Each camcorder views the three IBSs on the opposite end plate through a hole in the central plate which supports power and electrical systems.

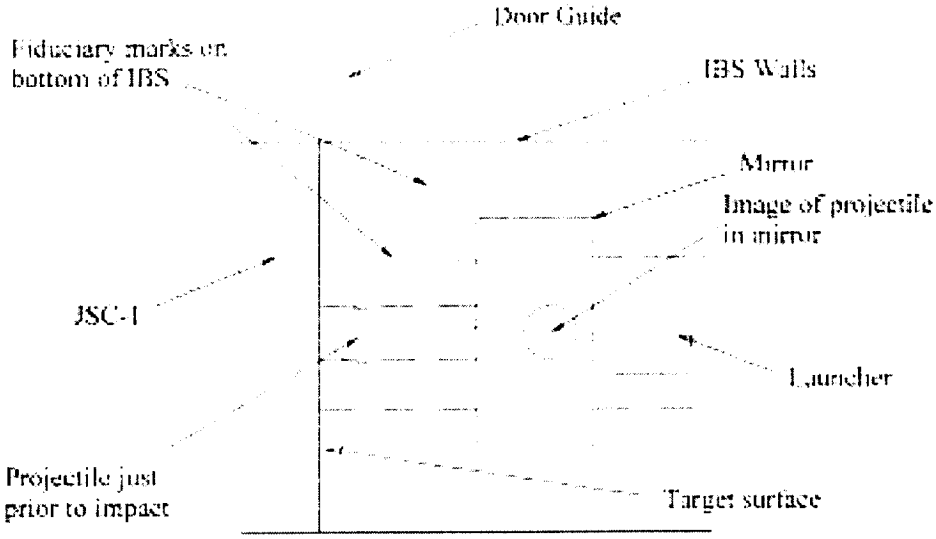

FIG. 2. A schematic of a COLLIDE Impactor Box System (IBS) from the same perspective as the camcorders. The target surface is viewed edge on, and an angled mirror provides an orthogonal view of the impact. The projectile travels from right to left, and illumination is from the right.

The experiment was powered by its internal set of 18 D-cell alkaline batteries. A baroswitch provided by NASA on the exterior of the Get Away Special canister (GASCAN) turned on the experiment as the Space Shuttle ascended through 50,000 feet. This began an internal 24-hr timer circuit. Astronaut activation of the experiment within the 24-hr time period following launch initiates the experiment. In the absence of an initiation within 24 hr after launch, the experiment auto-initiates.

COLLIDE was installed in its flight GASCAN on January 21, 1998, at the Kennedy Space Center. The GASCAN was evacuated to a pressure of 0.03 Torr prior to launch to prevent air currents from interfering with ejected dust trajectories and to more closely simulate the space environment being studied. Air filters were placed over venting holes at the back of each target tray to allow air in the pore spaces of the JSC-1 to evacuate so that no eruptions would occur due to an overpressure in the target material when the target tray door was removed in flight. The camcorders were contained in air-tight, sealed containers with glass viewports to prevent sticking of moving parts and evaporation of lubricants. COLLIDE was launched on the Space Shuttle Columbia's STS-90 mission on April 17, 1998. The astronauts sent a signal to initiate the experiment 27 hr and 45 min after launch. The astronauts confirmed successful operation of the baroswitch, and by this time, the internal timer circuit had already initiated the experiment. Columbia landed on May 3, 1998, at the shuttle landing facility at the Kennedy Space Center, and COLLIDE was removed from its GASCAN on May 18, 1998.

III. EXPERIMENTAL RESULTS

Three of the six IBSs operated nominally. Launch vibrations cracked the glass viewports of both camcorder sealed containers, resulting in an increase in the ambient pressure in the rest of the GASCAN to 19 Torr. The door mechanisms on two IBSs jammed, also due to misalignment induced by launch vibrations. The projectile in IBS 5 (designed for a launch speed of 1 cm/sec, Table I), never left the launcher due to internal friction in the launcher, though the launch mechanism activated properly. Video quality was poor on the first IBS recorded by each camcorder, but velocity information has been retrieved for each of these impacts. The actual impact velocities as measured from the flight tape are given in Table II for the five projectiles that launched. Table II also includes measured normal coefficients of restitution, $\varepsilon_n = v_n/v_i$, where v_n is the normal component of the rebound velocity, v_i is the impact velocity, and $1 - \varepsilon_n^2$ is the energy dissipated in a head-on collision between particles with

TABLE II
Normal Coefficient of Restitution

IBS	Projectile speed (cm/sec)	Door functioned	Focus	Normal rebound velocity (cm/sec)	Coefficient of restitution (ε_n)
1	14.80 ± 0.09	Yes	Yes	0.41 ± 0.02	0.028 ± 0.002
2	12.18 ± 0.14	No	Yes	6.86 ± 0.12	$0.56 \pm 0.01^*$
	6.6 ± 0.2			2.7 ± 0.2	$0.41 \pm 0.04^*$
3	28 ± 2.8	No	No	13 ± 1.3	$0.46 \pm 0.1^*$
4	17.10 ± 0.21	Yes	Yes	0.37 ± 0.02	0.022 ± 0.002
5	0	Yes	Yes	N/A	N/A
6	90 ± 15	Yes	No	2.8 ± 0.5	0.03 ± 0.01

Note. (*) rebound off painted aluminum door instead of JSC-1 powder. The projectile in IBS 2 bounced off the door a second time, allowing measurement of ε_n for two impact velocities. Uncertainties are standard deviations from linear regression fits to displacement measurements, except for IBS 3 and IBS 6, which are higher due to the poor image quality and are based on estimates of error in measuring position. ε_n is the ratio of the normal component of the rebound velocity to the impact velocity.

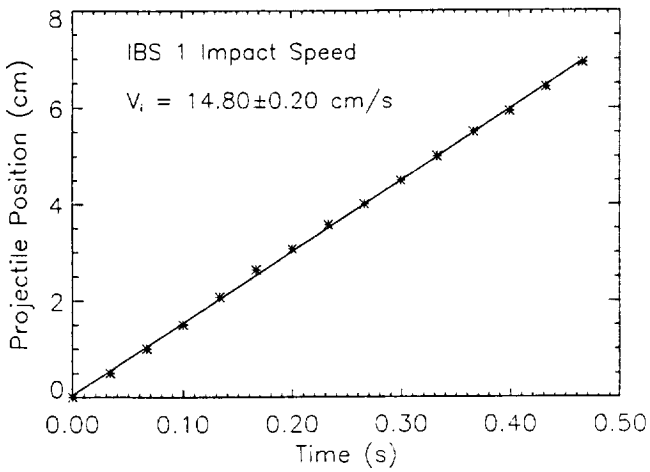

FIG. 3. Measured relative positions of the projectile in IBS 1 prior to impact with the JSC-1 target surface and a linear fit to the data. The linear fit and standard deviation provide the velocities and uncertainties in Table II.

no spin. We include ε_n for impacts onto the closed IBS doors to show the experimental scatter. The actual values of ε_n for the impacts onto the doors includes some small but unmeasured energy dissipation from movement of the door at impact. Projectile velocities were obtained by measuring the frame-by-frame position of the projectiles from the digital videotape. An example of the position data used to compute velocities is shown in Fig. 3.

Bridges *et al.* (1984) and Hatzes *et al.* (1988) performed impact experiments with frosted and unfrosted ice spheres at velocities less than 1 cm/sec and found a relationship between coefficient of restitution and impact speed. Dilley (1993) examined the functional dependence of the coefficient of restitution on particle size and mass, and Dilley and Crawford (1996) performed ice impact experiments at 1 cm/sec with different impactor masses. Supulver *et al.* (1995) performed normal and glancing collisions of ice spheres with an ice brick and measured normal and tangential coefficients of restitution. We show the data from COLLIDE in the context of these other low-velocity impact experiments in Fig. 4.

A concern prior to flight was that trapped air in the pore spaces of the sample would disturb the surface of the target powder. The videotape shows that on the four IBSs for which the doors opened fully, there was no disturbance to the target layer. The impactors made simple spherical depressions in the target layer, raising a small rim around the depression as the target dust was displaced by the impact. The teflon spheres rebounded off the powder surface at an angle, indicating that the spheres were spinning on impact and had a low tangential coefficient of restitution. Almost no ejecta was produced in any of the impacts, but some JSC-1 powder did stick to each projectile. Sample frames from IBS 4 are shown in Fig. 5. The spot of powder on the teflon sphere enables us to determine the rotation rate of the sphere after impact with the powder surface. The complete rotations of the projectile are visible in the mirror of IBS 4 and show that the rotation axis is parallel to the target surface. Similarly, by assuming that the sphere rolled through the launch tube with no slipping, we can place an upper limit on the initial rotation rate. This allows us to place a lower limit on the tangential coefficient of restitution, ε_t, which is given by (Araki and Tremaine 1986)

$$\mathbf{W}_t' = \varepsilon_t \mathbf{W}_t; \quad \varepsilon_t = \frac{\mathbf{V}_t' + r\omega' \times \hat{\lambda}}{\mathbf{W}_t}, \tag{3}$$

where r is the projectile radius, ω' is the rotation rate after impact, $\mathbf{V}_t'$ is the tangential component of the projectile velocity after impact, $\mathbf{W}_t$ ($\mathbf{W}_t'$) is the tangential velocity of the projectile surface prior to (after) impact, and $\hat{\lambda}$ is a unit vector normal to the target surface. We use estimated initial rotation rates to get $\mathbf{W}_t$, and video measurements to get $\mathbf{W}_t'$ and compute ε_t. These values are shown in Table III.

IV. CONCLUSIONS AND DISCUSSION

The impact experiments performed in COLLIDE are the first microgravity cratering experiments into regolith. Terrestrial impact experiments include hypervelocity ($v > 1$ km/sec) impact experiments which simulate the bombardment of planetary surfaces by micrometeoroids (e.g., Asada 1985, Gault 1973, Gault and Wedekind 1977, Gault *et al.* 1972, Hartmann 1985, Stöffler *et al.* 1975, Yamamoto and Nakamura 1997), intermediate velocity impact experiments (e.g., Hartmann 1978, Hartmann 1985,

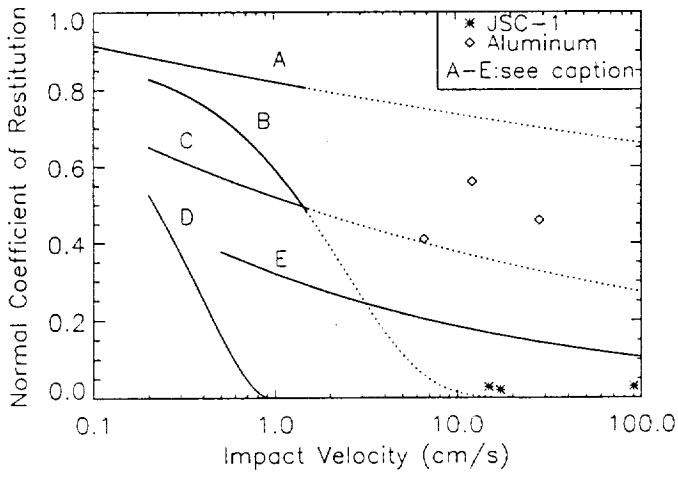

FIG. 4. Normal coefficients of restitution found in COLLIDE and functional fits to data obtained by other researchers for impacts between ice particles near 1 cm/sec. (*) Values from COLLIDE for impacts into JSC-1 powder. (◇) Values from COLLIDE for impacts into painted aluminum. For all model fits, a solid line is a functional fit to the data over the velocity range measured, and dotted lines are extrapolations of the functional fits to the velocities used in COLLIDE. (curve A) Fit to data of Hatzes *et al.* (1988) for impacts between smooth ice spheres at 0.2 to 1.5 cm/sec. (curve B) Fit to data of Hatzes *et al.* (1988) for impacts between frosted ice spheres at 0.2 to 1.5 cm/sec. (curve C) Fit to data of Supulver *et al.* (1995) for impacts between unfrosted ice surfaces. (curve D) Model of Dilley and Crawford (1996) fit to data for impacts of an ice sphere at 1 cm/sec for a projectile the size of the larger COLLIDE projectile. (curve E) Fit to data of Bridges *et al.* (1984) for impacts between unfrosted ice surfaces.

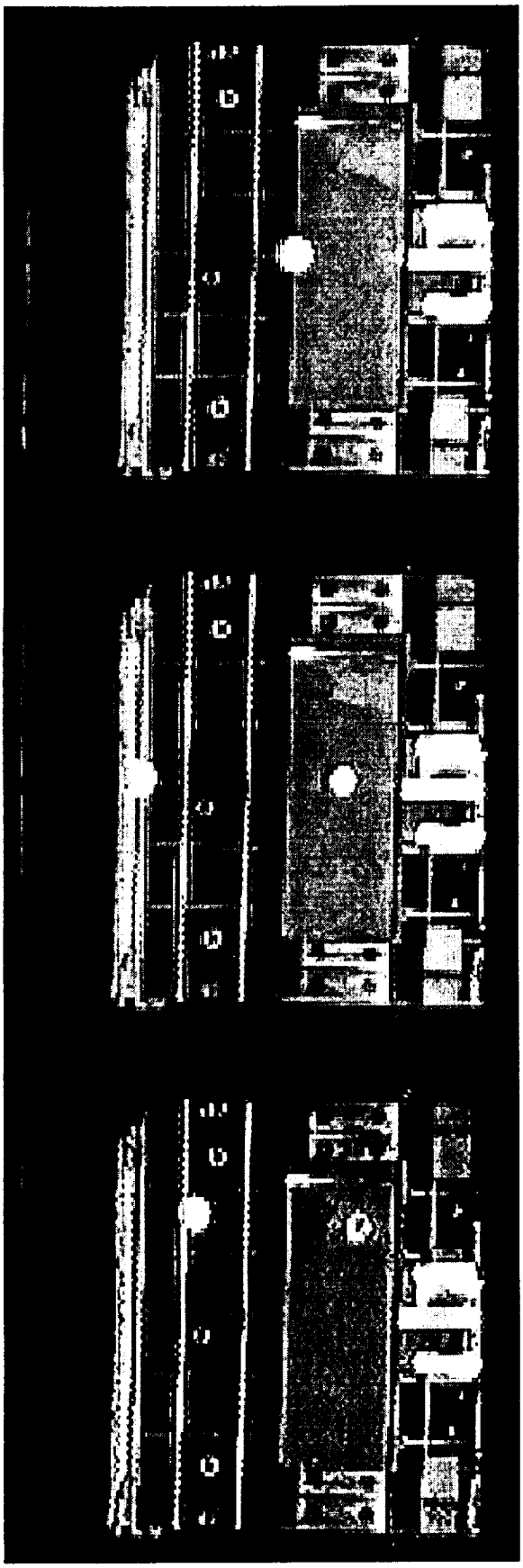

TABLE III
Tangential Coefficient of Restitution

IBS	Initial rotation rate[a] (sec^{-1})	Tangential rebound velocity (cm/sec)	Final rotation rate (sec^{-1})	Tangential coefficient of restitution[b] (ε_t)
1	31	0.39 ± 0.02	$3.49 \pm .24$	0.086
4	37	0.78 ± 0.02	$2.48 \pm .12$	0.023
6	94	4.8 ± 0.5	Unknown	-0.053^*

Note. Results are presented only for those impacts onto JSC-1 powder. (*) This lower limit is based on an assumed final rotation rate of 0. Because the impact was into a nonrotating target, the effective lower limit of $\varepsilon_t = 0$ for this impact.

[a] Initial rotation rates are upper limits assuming the projectile had zero slipping inside the launcher.

[b] Values are lower limits based on assumed initial rotation. Initial tangential velocity of the projectiles' surfaces was entirely due to rotation.

Ryan *et al.* 1991), and low-velocity ($\approx$1 cm/sec) pendulum experiments with ice impactors (Bridges *et al.* 1984, Hatzes *et al.* 1988, Supulver *et al.* 1995, Dilley and Crawford 1996). Extrapolation from the results of ejecta production from the Hartmann (1985) 5–12 m/sec impacts into regolith suggests that regolith could be produced at lower velocities, although the presence of a strong gravitational force might mask the phenomenon at lower energies. Results on ejecta from the hypervelocity experiments have been used with scaling theory to derive analytic expressions for the outcomes of hypervelocity impacts (e.g., Housen *et al.* 1983, Holsapple and Schmidt 1987, Holsapple 1993). The scaling is only valid for hypervelocity impacts, but in the absence of other models it has been used to extrapolate to the much lower collision velocities common in planetary rings and protoplanetary disks (e.g., Colwell and Esposito 1990a, 1990b, Canup and Esposito 1995, 1997, Throop and Esposito 1998). The types of collisions that occur between dust-covered objects in planetary rings are better suited to study with the techniques of granular mechanics (e.g., Pöschel and Buchholtz 1993, Buchholtz and Pöschel 1993) than hypervelocity impacts.

Although they are not directly comparable, an extrapolation to the fit to the data for frosted ice spheres of Hatzes *et al.* (1988) comes closest to matching the normal coefficients of restitution measured here (Fig. 4, curve B), though it underestimates ε_n by a factor of 10 at COLLIDE velocities. That curve is a fit to data obtained with a pendulum and a spherical impactor striking an ice brick, each with a thin layer of compacted frost. Their data were for impactor radii of curvature between 2.5 and 20 cm,

FIG. 5. Images from one of the COLLIDE impact experiments (IBS 4) showing the projectile prior to impact (top), at impact (middle), and after impact (bottom). The projectile's reflection is visible in the mirror, which is mounted to the bottom of the IBS in the bottom two panels. After impact, a spot of dust is visible on the reflected image of the projectile in the mirror. This was used to measure the post-impact rotation rate and the tangential coefficient of restitution. The spacing of the fiduciary grid lines on the bottom of the IBS is 2 cm.

compared to the 0.48 cm radius of our projectiles, and for impact speeds below 1.5 cm/sec. Their empirical fit includes a radius dependence:

$$\varepsilon_n(v, R) = 0.90 \exp[(0.01R - 0.41)v]. \quad (4)$$

Further experiments with impacts in the same velocity range as Hatzes *et al.* are needed to determine if a similar functional dependence on v and R holds for impacts into regolith like the higher velocity impacts presented here.

In a different type of impact experiment, Blum and Münch (1993) studied low-velocity (0.15–4 m/sec) impacts between small dust aggregates, and found rebound and fragmentation, but no accretion. In subsequent experiments, Wurm and Blum (1998) found efficient accretion of dust aggregates at speeds up to 1 cm/sec. Their experiments focused on the first stages of coagulation of dust in the protoplanetary nebula. In contrast, the experiments reported here assume that cm- to m-sized objects have already formed and look at the effects of collisions between such particles with regoliths. Results from COLLIDE show a near total absence of dust ejecta for collisions of 3/8 inch diameter teflon spheres into JSC-1 powder. The rebound velocities are less than the escape velocity for silicate bodies as small as 1 m in radius.

The kinetic energy of the three impacts into JSC-1 ranged from 10^2 to 3×10^4 erg. Hartmann (1985) performed impact experiments into basalt and pumice powders at speeds ranging from 5.3 to 2321 m/sec, with a minimum kinetic energy of 6.1×10^5 erg. In his low-velocity impacts, there was a measurable amount of ejecta (but less than the impactor mass) with ejecta velocities of 1 to 2 m/sec, when measurable. For his lowest energy impact into basalt powder, the ejecta mass was 2.1 g, the glass sphere impactor mass was 2.39 g, and the crater diameter was 4 cm. Values consistent with these were found in our own drop tests prior to launch of COLLIDE. Simple extrapolation of these results would suggest ejecta velocities in COLLIDE of several centimeters per second, with a potential for more abundant, slower ejecta due to the absence of gravity (typical vibrational accelerations in the Space Shuttle payload bay during normal activity are on the order 1 cm/sec^2). However, only one or two small clumps of ejecta were observed in the two COLLIDE impacts into JSC-1 for which video resolution is sufficient to identify ejecta, and these were apparently spun out of the surface by the spinning projectile. Ejecta velocities are generally higher in air than in low ambient pressure (Hartmann 1978), so the relatively high pressure inside COLLIDE does not explain the lack of ejecta.

Surface forces between grains of JSC-1 were strong enough to prevent the release of any dust in these low-energy collisions. The impacts in COLLIDE were below the energy threshold necessary to produce ejecta. The size of the impactor is an important parameter to vary in future experiments, along with impact velocity (Hatzes *et al.* 1988, Dilley 1993). Even at the low velocities studied with COLLIDE, if the impactors had been much more massive, enough target dust would have been displaced to potentially release a significant amount of ejecta. Further microgravity experiments into regolith are needed to identify the transition from the "clean" regime seen in the results presented here to the ejecta regime. This transition may be a function of regolith porosity, size distribution, impactor mass, and impactor velocity.

The collisions were approximately 3 to 5 times less elastic than an extrapolation to data fits for impacts between icy spheres (Fig. 4, curve E) commonly used in planetary ring simulations (e.g., Hänninen and Salo 1994, Spahn *et al.* 1995, Hertzsch *et al.* 1997). A difference is not surprising given the very different surface conditions between COLLIDE impacts (teflon spheres into JSC-1 powder) and those of Bridges *et al.* (1984), Hatzes *et al.* (1988), Supulver *et al.* (1995), and Dilley and Crawford (1996). Dilley's (1993) model predicts a much lower coefficient of restitution for smaller impactors (curve D in Fig. 3) which, coupled with the powder nature of our target material, helps explain the lower normal coefficients of restitution described here compared to the ice impacts shown in Fig. 4 which used larger impactors and a solid target. The normal coefficients of restitution found by COLLIDE are consistent, however, with the low values first seen by Hartmann (1978) in terrestrial drop impact experiments.

Even with the small gravitational force acting on the regolith targets in our experiment, virtually no ejecta was produced in these low-energy impacts. This confirms the earlier finding that accretion is favored by the presence of a regolith, and extends the result to collisions between even very small (low surface gravity) dust-covered objects in planetary rings and protoplanetary disks. Further experiments at even lower velocities are needed, where impacts tend to be much more elastic. Although the regolith particle size distribution and composition in COLLIDE are different from what exists in protoplanetary disks and planetary rings, the qualitative results should hold for different materials. Other experiments have been designed to study the earlier stage of accretion with sticking of individual dust grains to form larger aggregates (Wurm and Blum 1998, and CODAG, another GAS experiment which flew on STS-95 in October 1998 (J. Blum, personal communication)). While our results are favorable for the accretion of planetesimals, at least during the part of the accretion process with velocities in the 10–100 cm/sec range and assuming a substantial regolith, they raise questions about the amount of dust that is released in planetary rings by interparticle collisions. Observed dust rings may be primarily due to micrometeoroid bombardment of ring particles with a small or negligible contribution from interparticle collisions.

ACKNOWLEDGMENTS

This research was supported by NASA's Microgravity Research Division and the Innovative Research Program. Technical support from NASA's Shuttle Small Payloads Program office, Lewis Research Center, and the Kennedy Space Center is gratefully acknowledged. We than Larry Esposito and Mihály Horányi for valuable discussions and Bill Hartmann, Mark Bullock, and an anonymous referee for comments on the manuscript.

REFERENCES

Araki, S., and S. Tremaine 1986. The dynamics of dense particle disks. *Icarus* **65**, 83–109.

Asada, N. 1985. Fine fragments in high-velocity impact experiments. *J. Geophys. Res.* **90**, 12,445–12,453.

Barge, P., and R. Pellat 1991. Mass spectrum and velocity dispersions during planetesimal accumulation. *Icarus* **93**, 270–287.

Blum, J., and M. Münch 1993. Experimental investigations on aggregate–aggregate collisions in the early solar nebula. *Icarus* **106**, 151–167.

Bridges, F. G., A. P. Hatzes, and D. N. C. Lin 1984. Structure, stability, and evolution of Saturn's rings. *Nature* **309**, 333–335.

Buchholtz, V., and T. Pöschel 1993. A vectorized algorithm for molecular dynamics of short range interacting particles. *Int. J. Modern Phys. C* **4**, 1049–1057.

Canup, R. M., and L. W. Esposito 1995. Accretion in the Roche zone: Coexistence of rings and ringmoons. *Icarus* **113**, 331–352.

Canup, R. M., and L. W. Esposito 1997. Evolution of the G Ring and the population of macroscopic ring particles. *Icarus* **126**, 28–41.

Colwell, J. E., and L. W. Esposito 1990a. A numerical model of the uranian dust rings. *Icarus* **86**, 530–560.

Colwell, J. E., and L. W. Esposito 1990b. A model of dust production in the Neptune ring system. *Geophys. Res. Lett.* **17**, 1741–1744.

Dilley, J. P. 1993. Energy loss in collisions of icy spheres: Loss mechanism and size–mass dependence. *Icarus* **105**, 225–234.

Dilley, J. P., and D. Crawford 1996. Mass dependence of energy loss in collisions of icy spheres: An experimental study. *J. Geophys. Res.* **101**, 9267–9270.

Esposito, L. W. 1993. Understanding planetary rings. *Annu. Rev. Earth Planet. Sci.* **21**, 487–523.

Gault, D. E. 1973. Displaced mass, depth, diameter, and effects of oblique trajectories for impact craters formed in dense crystalline rocks. *Moon* **6**, 32–44.

Gault, D. E., and J. A. Wedekind 1977. Experimental hypervelocity impact into quartz sand II, effects of gravitational acceleration. In *Impact and Explosion Cratering* (D. J. Roccy, R. O. Peppin, and R. B. Merrill, Eds.), pp. 1231–1244. Pergamon, Elmsford, NY.

Gault, D. E., F. Hörz, and J. B. Hartung 1972. Effects of microcratering on the lunar surface. *Geochim. Cosmochim. Acta* **3**, 2713–2734.

Greenberg, R., W. K. Hartmann, C. R. Chapman, and J. F. Wacker 1978. The accretion of planets from planetesimals. In *Protostars and Planets* (T. Gehrels, Ed.), pp. 599–622. Univ. Arizona Press, Tucson.

Hänninen, J., and H. Salo 1994. Collisional simulations of satellite Lindblad resonances. *Icarus* **108**, 325–346.

Hartmann, W. K. 1978. Planet formation: Mechanism of early growth. *Icarus* **33**, 50–62.

Hartmann, W. K. 1985. Impact experiments. 1. Ejecta velocity distributions and related results from regolith targets. *Icarus* **63**, 69–98.

Hatzes, A. P., F. G. Bridges, and D. N. C. Lin 1988. Collisional properties of ice spheres at low impact velocities. *Mon. Not. R. Astron. Soc.* **231**, 1091–1115.

Hertzsch, J.-M., H. Scholl, F. Spahn, and I. Katzorke 1997. Simulation of collisions in planetary rings. *Astron. Astrophys.* **320**, 319–324.

Holsapple, K. A. 1993. The scaling of impact processes in planetary sciences. *Annu. Rev. Earth Planet. Sci.* **21**, 333–373.

Holsapple, K. A., and R. M. Schmidt 1987. Point-source solutions and coupling parameters in cratering mechanics. *J. Geophys. Res.* **92**, 6350–6376.

Housen, K. R., R. M. Schmidt, and K. A. Holsapple 1983. Crater ejection scaling laws: Fundamental forms based on dimensional analysis. *J. Geophys. Res.* **88**, 2485–2499.

McKay, D. S., J. L. Carter, W. W. Boles, C. C. Allen, and J. H. Allton 1994. JSC-1: A new lunar soil simulant. In *Engineering, Construction, and Operations in Space IV*, pp. 857–866. American Society of Civil Engineers.

Pöschel, T., and V. Buchholtz 1993. Static friction phenomena in granular materials: Coulomb law versus particle geometry. *Phys. Rev. Lett.* **71**, 3963–3966.

Ryan, E. V., W. K. Hartmann, and D. R. Davis 1991. Impact experiments 3: Catastrophic fragmentation of aggregate targets and relation to asteroids. *Icarus* **94**, 283–298.

Sandor, B. J., and R. T. Clancy 1995. Microwave observations and modeling of a lunar eclipse. *Icarus* **115**, 387–398.

Spahn, F., J.-M. Hertzsch, and N. V. Brilliantov 1995. The role of particle collisions for the dynamics in planetary rings. *Chaos, Solitons, Fractals* **5**, 1945–1964.

Stern, S. A. 1996a. Signatures of collisions in the Kuiper Disk. *Astron. Astrophys.* **310**, 999–1010.

Stern, S. A. 1996b. On the collisional environment, accretion time scales, and architecture of the massive, primordial Kuiper Belt. *Astron. J.* **112**, 1203–1211.

Stern, S. A., and J. E. Colwell 1997. Collisional erosion in the primordial Edgeworth–Kuiper Belt and the generation of the 30–50 AU Kuiper Gap. *Astrophys. J.* **490**, 879–882.

Stöffler, D., D. E. Gault, J. Wedekind, and G. Polkowski 1975. Experimental hypervelocity impact into quartz sand: Distribution and shock metamorphism of ejecta. *J. Geophys. Res.* **80**, 4062–4077.

Supulver, K. D., F. G. Bridges, and D. N. C. Lin 1995. The coefficient of restitution of ice particles in glancing collisions: Experimental results for unfrosted surfaces. *Icarus* **113**, 188–199.

Throop, H. B., and L. W. Esposito 1998. G Ring particle sizes derived from ring plane crossing observations. *Icarus* **131**, 152–166.

Weidenschilling, S. J., and J. N. Cuzzi 1993. Formation of planetesimals in the solar nebula. In *Protostars and Planets III* (E. H. Levy and J. I. Lunine, Eds.), pp. 1031–1060. Univ. Arizona Press, Tucson.

Weidenschilling, S. J., C. R. Chapman, D. R. Davis, and R. Greenberg 1984. Ring particles: Collisional interactions and physical nature. In *Planetary Rings* (R. Greenberg and A. Brahic, Eds.), pp. 367–415. Univ. Arizona Press, Tucson.

Wurm, G., and J. Blum 1998. Experiments on preplanetary dust aggregation. *Icarus* **132**, 125–136.

Yamamoto, S., and A. M. Nakamura 1997. Velocity measurements of impact ejecta from regolith targets. *Icarus* **128**, 160–170.